Taher *et al. Renewables (2015) 2:15*
DOI 10.1186/s40807-015-0015-z

Renewables: Wind, Water, and Solar
a SpringerOpen Journal

ORIGINAL RESEARCH Open Access

Dual effect of TiO_2 and Co_3O_4 co-semiconductors and nanosensitizer on dye-sensitized solar cell performance

F. A. Taher[1*], Galila M. El-sayed[1], N. M. Khattab[2] and N. Almohamady[3]

Abstract:
Dye-sensitized solar cell (DSSC) was fabricated using nanosize of the dye sensitizer (Alizarin Yellow, AY) that was prepared by ball milling. The particle size and the composition of nano-Alizarin Yellow (nAY) was investigated using TEM and ^{1}H- and ^{13}C-NMR spectra, respectively. The effect of sensitizer size reduction on DSSC efficiency was studied. Co_3O_4 as a semiconductor in DSSC was prepared and confirmed by XRD. Also, composite of TiO_2 and Co_3O_4 was used to improve the DSSC efficiency. In addition, the effect of terpineol as a solvent was tested. Photocurrent–photovoltage curves of all prepared DSSCs were investigated. Finally, to test the validity of the results, standard error was calculated.

Keywords: DSSC, Co_3O_4@TiO_2 nanocomposites, Nanosensitizer, Alizarin Yellow

Background

DSSC is an alternative solution for the future energy crisis as a productive source for renewable energy (Kato et al. 2011; Zhuiykov 2014; Ludin et al. 2014). Excitation of dye sensitizer that was doped onto semiconductor or co-semiconductor by sun radiation to generate an electron and leave behind a hole is the initial photon-induced electron reaction in DSSC (Yum et al. 2014). After transition of the excited electron from semiconductor conduction band to a counter electrode through working electrode, the ground state of the dye is reached by electrolyte oxidation (Choi et al. 2013; Han and Ho 2014). The main issue is in returning some electrons back to the dye ground state or electrolyte causing an increase in the electron–hole recombination rate and then deficiency in DSSC efficiency (Lai et al. 2008; Akpan and Hameed 2009; Yamaguchi et al. 2010; Reda 2010; Kato et al. 2011; Tian et al. 2010; Kantonis et al. 2011; Sharma et al. 2010; Basheer et al. 2014a, b). Since, the efficiency of the DSSC relies on the sensitizer and semiconductor, the idea here is to increase the absorption band of the sensitizer by increasing its surface area or decrease the electron–hole recombination rate using darker co-semiconductor to achieve higher solar conversion efficiency.

Actually, Im and his co-worker have used the cocktail effect of TiO_2 and Fe_2O_3 to increase the performance of DSSC. The efficiency of the DSSC has been developed by over 300 % (Im et al. 2011). Also, NiO/TiO_2 nanocomposites were prepared and used as modified photoelectrodes in quasi-DSSC with 2.29 % conversion efficiency as by Mekprasart et al. (2011). To the best of our knowledge, so far, the effect of Co_3O_4 as a co-semiconductor was not previously reported therein. In this work, the dye sensitizer was converted to nanosize to investigate its size reduction on the DSSC efficiency. Also, a composite of TiO_2 and Co_3O_4 was prepared to use as a semiconductor in DSSC. In addition, the effect of terpineol as a solvent was tested via I–V characteristic curves.

Methods

Preparation of nanodye

The chemical structure of Alizarin Yellow (AY, Dye-Star) is shown in Fig. 1. Nano-Alizarin Yellow, nAY, was

*Correspondence: Fatmataher@azhar.edu.eg
[1] Department of Physical Chemistry, Faculty of Science (Girls), Al-Azhar University, Youssif Abbas St., Nasr city, Cairo, Egypt
Full list of author information is available at the end of the article

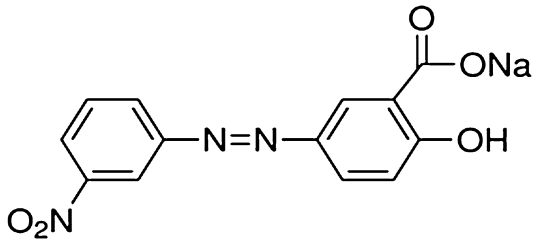

Fig. 1 Chemical structure of Alizarin Yellow (AY)

prepared by ball milling machine for 8 h (RETSCH PM 400, Germany), then heated at 40 °C for 24 h. The chemical composition of nAY was confirmed by ^{1}H- and ^{13}C-NMR spectroscopy (Bruker High-Performance Digital FT-NMR Spectrometer Avance III 400 MHz). TEM was measured to determine the particle size of nAY and its distribution (JEOL, TEM-1230).

Preparation of nanocobalt oxide

Cobalt oxide nanopowder was obtained by co-precipitation method. Drops of 0.3 M sodium hydroxide aqueous solution (98 %, Adwic) was stirred with aqueous solution of 0.01 M cobaltous chloride hexahydrate (98 %, Indiamart) for 2 h at room temperature. The obtained green precipitate, $Co(OH)_2$, was washed several times with distilled water. Nanocobalt oxide (Co_3O_4) was obtained after drying at 80 °C and sintering at 900 °C. All theses steps can be represented by the following equations:

$$2NaOH_{(aq)} + CoCl_2 \cdot 6H_2O_{(aq)} \rightarrow 2NaCl_{(aq)} + Co(OH)_2 \cdot 6H_2O_{(aq)}$$

$$Co(OH)_2 \cdot 6H_2O \xrightarrow{\triangleq 80^{\circ}C} Co(OH)_2 + 6H_2O$$

$$Co(OH)_2 \xrightarrow{\triangleq 900^{\circ}C} Co_3O_4 + H_2O$$

Accordingly, the crystalline structure of Co_3O_4 was confirmed by powder X-ray diffraction (XRD: Empyrean, Holland). To obtain the particle size of Co_3O_4 and its distribution, TEM measurement was conducted (JEOL, TEM-1230).

Preparation of Co_3O_4@TiO_2 composite

1.6 g Co_3O_4 and 5 g TiO_2 (anatase 99.7 %, P25, Sigma-Aldrich) were mixed with 25 ml distilled water, and stirred for 48 h at room temperature. The resultant complex was sintered at 600 ℃ for 1 h.

Preparation of TiO_2 and Co_3O_4@TiO_2 pastes

To prepare the pastes, 2 g TiO_2 and 2 g Co_3O_4@TiO_2 composite were separately added into a solution of 0.5 g polyethylene glycol (20,000 g/mol, Sisco) dissolved in 7 ml of distilled water (as a binder to prevent the film from cracking during drying), 5 ml ethanol, and 15 ml terpineol (Sigma-Aldrich). The resultant two mixtures were thermally heated at 100 °C for 6 h.

Preparation of the working electrode

Fluorine-doped tin oxide glass (FTO, Pilkington Kappa Energy, 18 Ω/cm^2) was cleaned with 95 % ethanol, 1-propanol and distilled water, then left to dry in open air. Before applying TiO_2 and Co_3O_4@TiO_2 pastes, FTO glass was heated in 0.2 M $TiCl_4$ solution (99 %, Merck) at 70 °C for 30 min to make a nanocrystalline TiO_2 film which prevents the electrolyte from approaching the conductive layer preventing the cell from the dark current. The previous pastes were coated onto FTO by the doctor blade technique using Scotch adhesive tape (thickness: 50 μm). The film was air dried for 10 min at room temperature and then annealed and sintered at 450 ℃ for 30 min. The loaded pastes on FTO were separately immersed in an aqueous solution of 1×10^{-4} M AY and 1×10^{-4} M nAY. The resultant working electrode was dried at room temperature overnight.

Preparation of the counter electrode

FTO glass was coated with Pt paste (Platisol, Solaronix) then dried at 70 °C for 3 h and sintered for 30 min at 450 °C under airflow of 30 ml/min. The counter electrode was then left to cool down to room temperature before usage.

Assembly of the DSSC

Between the counter and the working electrodes, the iodide/iodine electrolyte solution (0.5 M potassium iodide mixed with 0.05 M iodine in water-free ethylene glycol) was located and then binder clipped to immobilize each part. The area of the DSSC was fixed to be 2.25 cm^2.

Measurement of the photophysical and electrochemical properties

UV–Vis spectrophotometer was used to record the absorption spectra of AY, nAY, TiO_2 and Co_3O_4@TiO_2 solutions; emission spectra of AY and nAY solutions; and photoluminescence spectra of AY, nAY, AY–TiO_2 and nAY–TiO_2 solutions (Perkin Elmer, lambada 35, USA). I–V characteristics were measured using a photocurrent–voltage (I–V) curve analyzer (Peccell Technologies, Inc., PECK2400-N, version 2.1) under AM 1.5 (950 mW/cm^2) irradiation with a solar simulator (Peccell Technologies, PEC-L11).

Results and discussion

Effect of the size reduction on the characteristics of nAY

The effect of size reduction on the particle size, chemical composition and spectral analyses was investigated by TEM image, NMR and UV–Vis spectra, respectively. Figure 2 shows TEM photograph of the as prepared nAY. A homogenous rod-like structure was observed with diameters and lengths less than 20 and 100 nm, respectively.

To confirm whether the ball milling process results in the partial decomposition of some AY molecules or not, the ^{1}H- and ^{13}C-NMR spectra of nAY were measured (Fig. 3). As can be seen in Fig. 3a, the aromatic ring protons multiplet of nAY molecule were observed from 7.11 to 8.70 ppm. The resonance signal due to OH proton singlet was observed at 9.80 ppm. While for the corresponding carbon resonance, Fig. 3b, the carbonyl carbon signal appears in a characteristic field of 146.02 ppm which confirms that there is no partial chemical decomposition of nAY molecule and the ball milling process does not affect its composition.

UV–Vis absorption spectra were obtained from nAY and AY solution (Fig. 4). When comparing the maximum absorption wavelength, λ_{max}, a bit of bathochromic shift of AY λ_{max} from 400 to 445 nm for nAY was observed which corresponds to the transition from HOMO to LUMO. This red shift of λ_{max} of nAY can be attributed to its smaller particle size (17–35 nm) that reflects a strong electron donation ability of nAY (increasing the delocalization of the π* orbital of AY), i.e., the absorption energy was shifted to lower frequency with decrease of the particles' diameter. This was readily observed from the reflected color change of AY from brilliant yellow to mustard yellow of nAY passing through canary yellow, where each color corresponds to the different particle size of nAY. After sensitization of AY and nAY on TiO_2, λ_{max} was shifted to red region by 100 and 55 nm, respectively, due to J-aggregation on TiO_2 surface (curves not inserted). In addition, the emission spectra of AY and nAY at 300 nm showed a broad spectral peak at the same position corresponding to relaxation to lower energy level (Fig. 5). Also, the lower emission intensity of nAY indicates the delay in recombination rate of e− and h^+ that emphasizes the advantage of using nAY in DSSC fabrication. This can also be noticed in the hypochromic shift of the photoluminescence spectra of AY to lower intensity for nAY (Fig. 6). This hypochromic effect indicates the decrease of photons number coming from electrons and holes recombination (Balraju et al. 2010). In addition, the adsorption of AY and nAY on TiO_2 showed the decrease in these photons numbers.

Characteristics of Co_3O_4

The X-ray diffraction characteristic peaks in Fig. 7a were analyzed to determine the structure and crystallite size of the as-prepared Co_3O_4. Nanopowder XRD peaks of Co_3O_4 are well consistent with the data of the JCPDS file (card no. 78-1970) of phase-pure Co_3O_4 with cubic spinel structure (Co^{2+} ions occupy the tetrahedral sites and Co^{3+} ions the octahedral sites) showing the main Bragg's reflection peak in the (311) plane. The peaks at 2θ value of 18.9°, 31.2°, 36.9°, 38.6°, 44.7°, 55.6°, 59.4° and 65.1° correspond to the crystal planes of (111), (220), (311), (222), (400), (422), (511) and (440) of well-crystallized Co_3O_4, respectively (Xiao et al. 2014; Kong et al. 2014). It is clear that Co_3O_4 is the only phase after the decomposition of the green precipitate, $Co(OH)_2$, at 900 °C without any other diffraction peak. The crystal size of Co_3O_4 is deduced through (311) plane using Scherrer equation $D = 0.94\,\lambda/\beta\cos\theta$ where D is the crystal size of Co_3O_4, λ is the wavelength of incident X-ray (0.154 nm), θ is the half diffraction angle of peak in degree, and β is

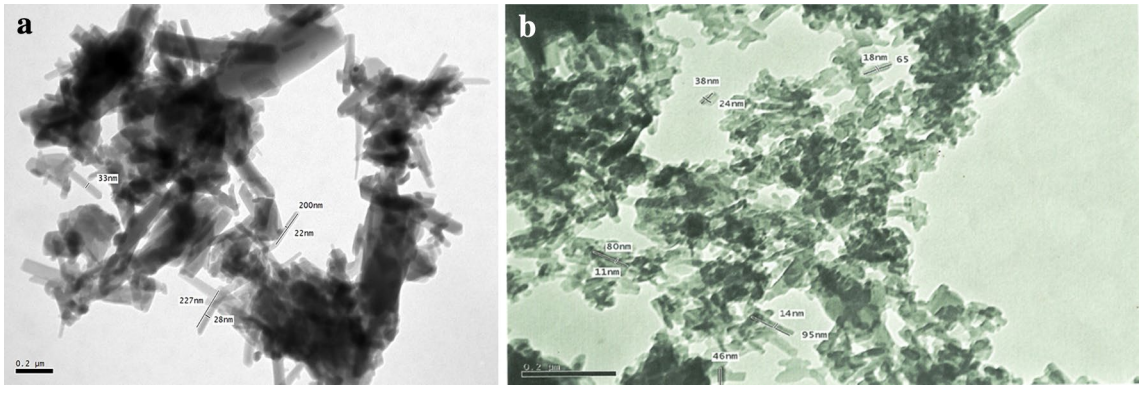

Fig. 2 TEM image of **a** AY and **b** nAY

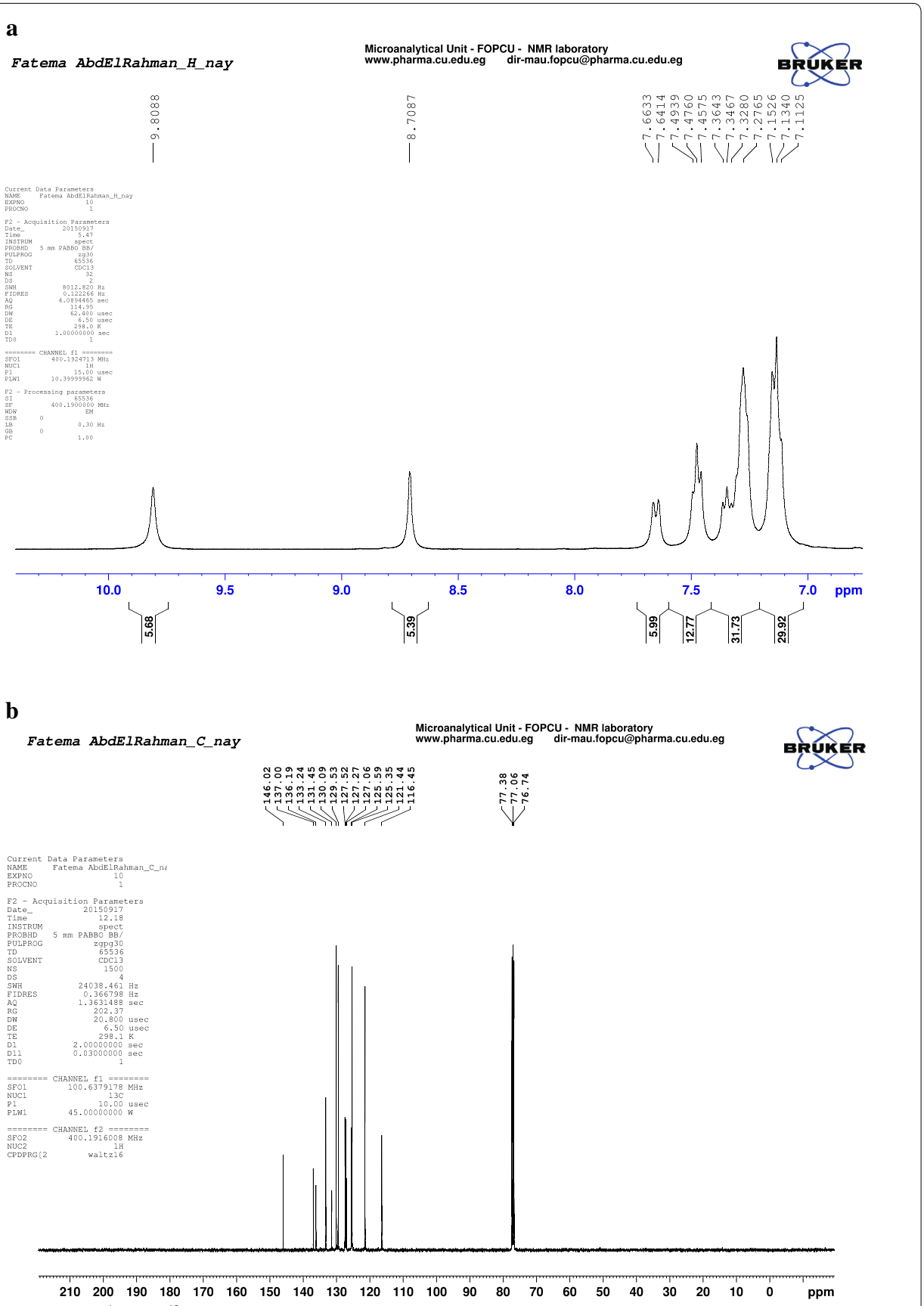

Fig. 3 Experimental **a** ^{1}H and **b** ^{13}C NMR spectra of nAY in CDCl3

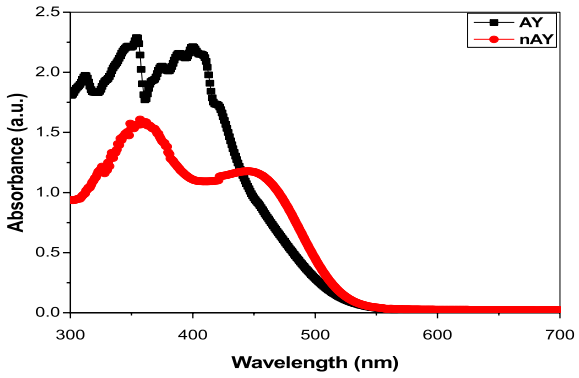

Fig. 4 UV–Vis absorption spectra of AY and nAY

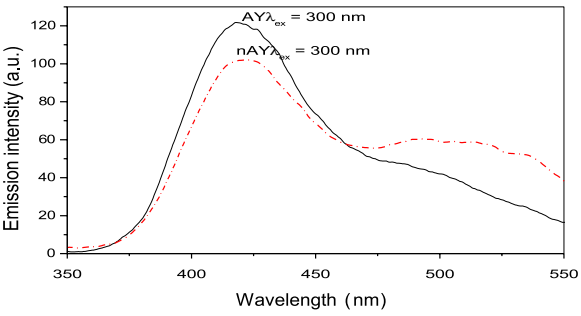

Fig. 5 Emission spectra of AY and nAY

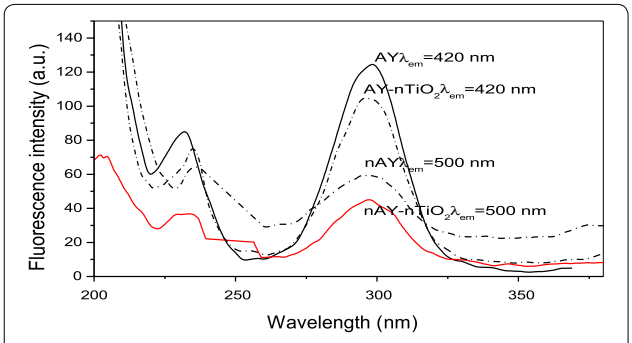

Fig. 6 Photoluminescence spectra for AY, nAY, AY–TiO_2 and nAY–TiO_2

the full width half maximum of a reflection located at 2θ. The average crystal size of Co_3O_4 is 154 nm which in a good agreement with TEM result of the cubic Co_3O_4 nanoparticles (Fig. 7b). Furthermore, the UV–Vis absorption spectra of TiO_2 and Co_3O_4@TiO_2 composite, Fig. 8, showed a band gap of 3.2 eV of the absorption band of TiO_2. Co_3O_4@TiO_2 composite exhibits a continuous absorption band of the dark composite toward higher wavelength in the range 300–750 nm (Kim et al. 2014). This red shift of the edge of the absorption peak implies band gap narrowing. The smaller band gap reflects the advantage of using Co_3O_4 in decreasing the recombination rate of e^- and h^+. The electrons that would transfer to the electrolyte or dye (AY or nAY) can be confined in the conduction band of Co_3O_4@TiO_2 composite (i.e., Co_3O_4@TiO_2 composite captures electrons from TiO_2 conduction band).

Photocurrent–voltage behavior of the DSSCs

Three effects of photosensitizer size reduction, nAY, oxide co-semiconductor, Co_3O_4, and presence of terpineol as a solvent on the efficiency of the prepared DSSCs

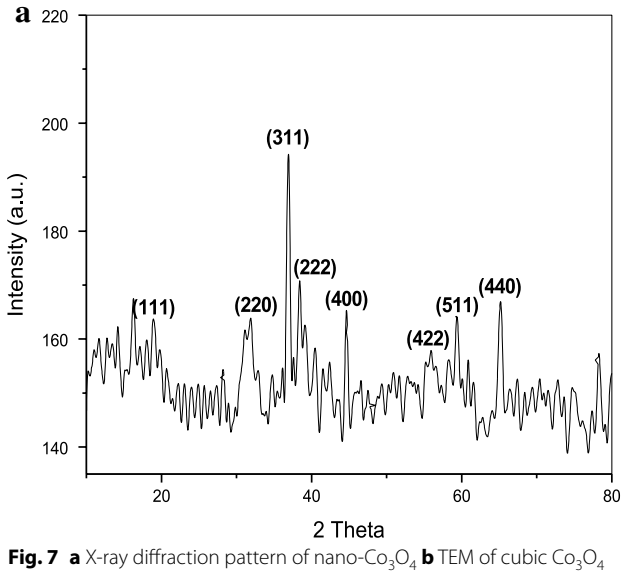

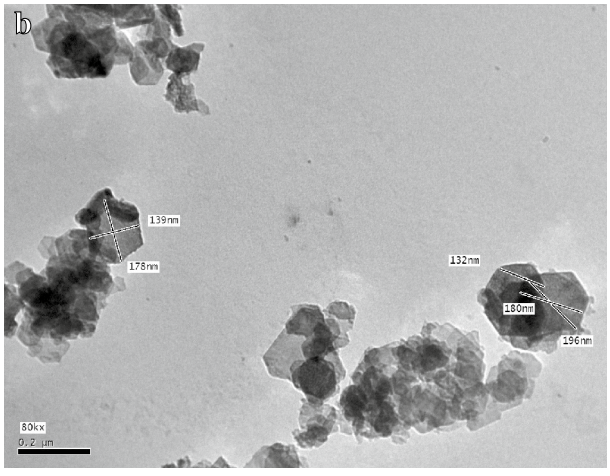

Fig. 7 **a** X-ray diffraction pattern of nano-Co_3O_4 **b** TEM of cubic Co_3O_4

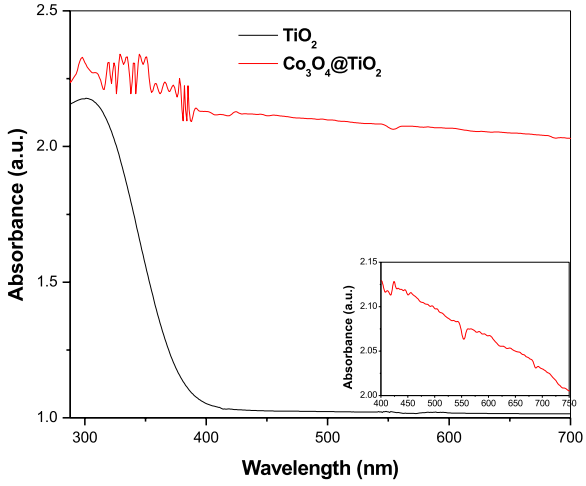

Fig. 8 UV–Vis absorption spectra of TiO_2 and Co_3O_4@TiO_2 composite

were investigated under 950 mW/cm^2 by analyzing their photocurrent density–voltage curves in Fig. 9 with error bars of photocurrent density. As for a comparison, the photovoltaic properties of the solar cells fabricated with commercial dye, AY, and its nanosize, nAY, in absence and presence of Co_3O_4 on the working electrode were measured. The values of open-circuit photovoltage, V_{oc}, short-circuit photocurrent, I_{sc}, fill factor *FF* and overall energy conversion efficiency are presented in Table 1.

The reduction of the original macro-size of AY to less than 100 nm of nAY, Fig. 2, has a great effect on the DSSC efficiency that increased by 70 % (C). This could be related to the nanosize of AY. As the size of a dye crystal decreases to nanometer regime, the size of AY particles begin to modify the properties of the crystal, so the electronic structure is altered from the continuous electronic bands to discrete or quantized electronic levels. Therefore, the nanomaterial becomes size dependent, and the electronic excitations shift to higher energy, and the oscillator strength is concentrated into just a few transitions. Actually, the presence of Co_3O_4 as a co-semiconductor in DSSCs electrode (B and D) increased their efficiency by 165 and 620 times in comparison with DSSC (A), respectively. This can be explained due to (1) TiO_2–Co_3O_4 composite that is darker in color and has a high absorption in the visible region of the solar spectrum. (2) The hexagonal crystal structure of Co_3O_4 which is a *p*-type semiconductor due to O_2-deficiency in its lattice and consequently the electron charge is fast injected into the conduction band (CB) of Co_3O_4. (3) Co_3O_4 shows different types of band gaps: *direct allowed* 2.06 and 1.44 eV, *direct forbidden* 1.38 and 1.26 eV, *indirect allowed* 1.10 eV (energy of phonon assisting indirect transition = 0.02) and *indirect forbidden* 0.75 eV (energy of phonon assisting indirect transition = 0.27) (Kabre 2011). The efficiency of DSSC (D) increased by 13-fold in the presence of terpineol as a solvent (E). It can be seen that the film prepared using terpineol as the solvent has exhibited the highest energy conversion efficiency. When water was used as the solvent, only polyethylene glycol exhibited a stable film formation on FTO conductive glass. This exhibited a cracked surface that was recognized by naked eye observation. On the other hand, when terpineol—an organic solvent with the hydroxyl functionalities that can accept or donate hydrogen bonds—was used as solvent, most of the semiconductor dispersions enabled us to form uniform thin films. Accordingly, the increased gap between ground state of dye and redox potential electrolyte would lead to higher performances of DSSCs in the following direction: (A) < (C) < (B) < (D) < (E). Figure 10 shows the standard error (SE) of the photocurrent density mean of DSSCs (A–E) to test the validity. A valid mean is reliable mean if it is at least 2.5 times standard deviation (Bevington and Robinson 2002). However, by calculating the DSSCs efficiency and considering these

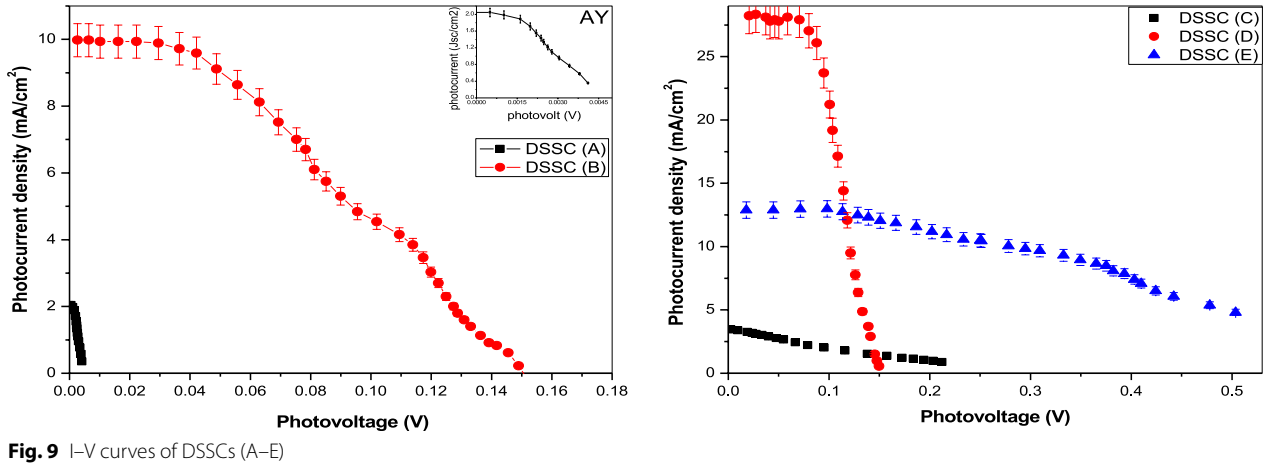

Fig. 9 I–V curves of DSSCs (A–E)

Table 1 The cell performance parameters of the prepared DSSCs

DSSCs	Dye	Semiconductor	Solvent	*Voc* (V)	*Isc* (mA)	SE (±)	FF	*η* (%)
A	AY	TiO_2	–	0.0041	2.0464	0.1482	0.3767	0.0033
B	AY	Co_3O_4@TiO_2	–	0.1489	9.9752	0.6135	0.3546	0.5548
C	nAY	TiO_2	–	0.2120	3.4553	0.1986	0.3040	0.2344
D	nAY	Co_3O_4@TiO_2	–	0.1496	28.2245	2.1594	0.4670	2.0765
E	nAY	Co_3O_4@TiO_2	Terpineol	0.5036	12.8855	0.4437	0.3458	2.3625

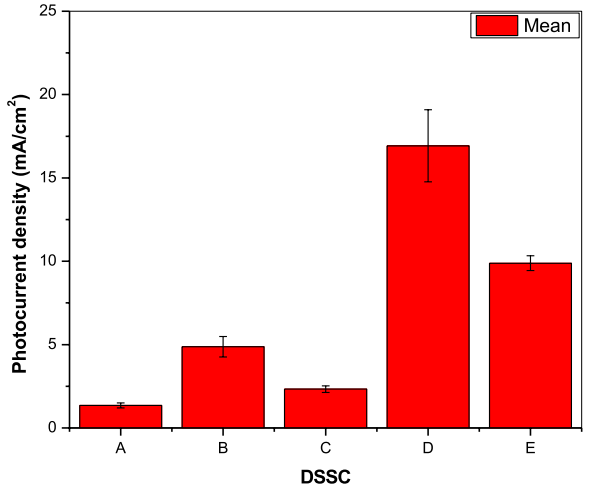

Fig. 10 Standard error analysis of photocurrent density of DSSCs (A–E)

standard errors values, it was found the efficiency values did not change for four digits.

The predicted mechanism for the conversion of photons to current for the DSSCs could be interpreted to pass through the following stages, Fig. 11. The electrons are excited by solar energy from HOMO to LUMO level of dye (AY/AY^+) that is adsorbed on TiO_2–Co_3O_4 composite surface, owing to the intermolecular π–π^* transition (Stage 1). These excited electrons diffuse immediately into the CB of TiO_2 (Stage 2); then move to the CB of Co_3O_4 (Stage 3) which decrease the electrons flow back to the HOMO (Stage 4) or I_3^- electrolyte in recombination (Stage 5) (i.e., reduce the electron trapping effect—by increasing the contact surface area of the TiO_2–Co_3O_4 composite with AY or electrolyte) (Anta 2012). These electrons go forward to the FTO of the working electrode (Stage 6). Consequently, these electrons reach the counter electrode through the external wiring (Stage 7). The oxidized dye (AY^+) accepts electron from I^- redox mediator, regenerating the HOMO of the dye (AY) and I^- is oxidized to I_3^-. The oxidized redox mediator, I_3^-, is reproduced to I^- at the counter electrode.

Conclusion

Five DSSCs were prepared to investigate the effects of their construction on their solar conversion efficiency. The nanosize of AY (less than 100 nm) has a great effect on the DSSC efficiency that increased by 70 %. Actually,

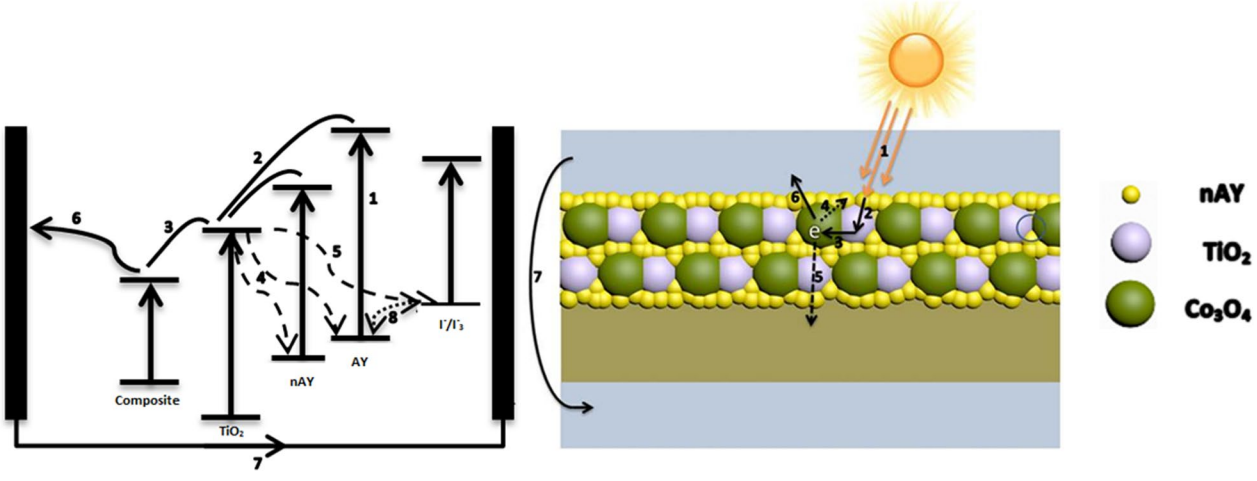

Fig. 11 DSSCs' predicted conversion mechanism

the presence of Co_3O_4 as a co-semiconductor in DSSCs electrode increased their efficiency by 165 and 620 times for the cells modified by $TiO_2 + Co_3O_4$ only and $TiO_2 + Co_3O_4$ with nAY, respectively. The presence of solvent (terpineol) increased the efficiency of DSSC by 13-fold. Finally, the predicted mechanism for the conversion of photons to current for the DSSCs was discussed.

Authors' contributions

FAT carried out the electrochemical studies of the DSSCs, participated in the sequence alignment, and drafted the manuscript and also the revision process. GME conceived the study, and participated in its design and helped to draft the manuscript. NK measured all the photophysical properties of DSSC, also participated in the study design and coordination. NA prepared all the as-obtained compounds and assembled the DSSCs. All authors read and approved the final manuscript.

Author details

[1] Department of Physical Chemistry, Faculty of Science (Girls), Al-Azhar University, Youssif Abbas St., Nasr city, Cairo, Egypt. [2] Solar Energy Department, National Research Center, El-bohooth St., Dokki, Giza, Egypt. [3] Faculty of Science (Girls), Youssif Abbas St., Nasr city, Cairo, Egypt.

Competing interests

The authors declare that they have no competing interests.

Received: 30 May 2015 Accepted: 16 October 2015
Published online: 04 November 2015

References

Akpan, U. G., & Hameed, B. H. (2009). Parameters affecting the photocatalytic degradation of dyes using TiO_2-based photocatalysts: a review. *Journal of Hazardous Materials, 170*(2), 520–529.

Anta, J. A. (2012). Electron transport in nanostructured metal–oxide semiconductors. *Current Opinion in Colloid & Interface Science, 17*(3), 124–131.

Balraju, P., Kumar, M., Deol, Y. S., Roy, M. S., & Sharma, G. D. (2010). Photovoltaic performance of quasi-solid state dye sensitized solar cells based on perylene dye and modified TiO_2 photo-electrode. *Synthetic Metals, 160*(1), 127–133.

Basheer, B., Mathew, D., George, B. K., & Nair, C. R. (2014a). An overview on the spectrum of sensitizers: the heart of dye sensitized solar cells. *Solar Energy, 108*, 479–507.

Basheer, B., Mathew, D., George, B. K., & Nair, C. R. (2014b). An overview on the spectrum of sensitizers: the heart of dye sensitized solar cells. *Solar Energy, 108*, 479–507.

Bevington, P. R., & Robinson, D. K. (2002). *Data reduction and error analysis for the physical sciences* (III ed.). New York: McGraw–Hill.

Choi, H., Nahm, C., Kim, J., Kim, C., Kang, S., Hwang, T., & Park, B. (2013). Review paper: toward highly efficient quantum-dot and dye-sensitized solar cells. *Current Applied Physics, 13*, S2–S13.

Han, N., & Ho, J. C. (2014). One-dimensional nanomaterials for energy applications. In S. C. Tjong (Ed.), *Nanocrystalline materials: their synthesis-structure-property relationships and applications* (II ed., pp. 75–120). USA: Elsevier.

Im, J. S., Lee, S. K., & Lee, Y. S. (2011). Cocktail effect of Fe_2O_3 and TiO_2 semiconductors for a high performance dye-sensitized solar cell. *Applied Surface Science, 257*(6), 2164–2169.

Kabre, T. S. (2011). *Co3O4 thin films: sol-gel synthesis, electrocatalytic properties and photoelectrochemistry*. **(Ohio: M.Sc. thesis)**.

Kantonis, G., Stergiopoulos, T., Katsoulidis, A. P., Pomonis, P. J., & Falaras, P. (2011). Electron dynamics dependence on optimum dye loading for an efficient dye-sensitized solar cell. *Journal of Photochemistry and Photobiology A: Chemistry, 217*(1), 236–241.

Kato, N., Higuchi, K., Tanaka, H., Nakajima, J., Sano, T., & Toyoda, T. (2011). Improvement in long-term stability of dye-sensitized solar cell for outdoor use. *Solar Energy Materials and Solar Cells, 95*(1), 301–305.

Kim, H. S., Kim, D., Kwak, B. S., Han, G. B., Um, M. H., & Kang, M. (2014). Synthesis of magnetically separable core@ shell structured $NiFe_2O_4$@ TiO_2 nanomaterial and its use for photocatalytic hydrogen production by methanol/water splitting. *Chemical Engineering Journal, 243*, 272–279.

Kong, C., Min, S., & Lu, G. (2014). Dye-sensitized cobalt catalysts for high efficient visible light hydrogen evolution. *International Journal of Hydrogen Energy, 39*(10), 4836–4844.

Lai, W. H., Su, Y. H., Teoh, L. G., & Hon, M. H. (2008). Commercial and natural dyes as photosensitizers for a water-based dye-sensitized solar cell loaded with gold nanoparticles. *Journal of Photochemistry and Photobiology A: Chemistry, 195*(2), 307–313.

Ludin, N. A., Mahmoud, A. A. A., Mohamad, A. B., Kadhum, A. A. H., Sopian, K., & Karim, N. S. A. (2014). Review on the development of natural dye photosensitizer for dye-sensitized solar cells. *Renewable and Sustainable Energy Reviews, 31*, 386–396.

Mekprasart, W., Noonuruk, R., Jarernboon, W., & Pecharapa, W. (2011). Quasi-solid-state dye-sensitized solar Cells Based on TiO_2/NiO core-shell nanocomposites. *Journal of Nanoscience and Nanotechnology, 11*(7), 6483–6489.

Reda, S. M. (2010). Synthesis of ZnO and Fe2O3 nanoparticles by sol–gel method and their application in dye-sensitized solar cells. *Materials Science in Semiconductor Processing, 13*(5–6), 417–425.

Sharma, G. D., Suresh, P., & Mikroyannidis, J. A. (2010). Quasi solid state dye-sensitized solar cells with modified TiO_2 photoelectrodes and triphenylamine-based dye. *Electrochimica Acta, 55*(7), 2368–2372.

Tian, H., Yang, X., Cong, J., Chen, R., Teng, C., Liu, J., et al. (2010). Effect of different electron donating groups on the performance of dye-sensitized solar cells. *Dyes and Pigments, 84*(1), 62–68.

Xiao, S., Cui, J., Yi, P., Yang, Y., & Guo, X. (2014). Insight into electrochemical properties of Co_3O_4-modified magnetic polymer electrolyte. *Electrochimica Acta, 144*, 221–227.

Yamaguchi, T., Tobe, N., Matsumoto, D., Nagai, T., & Arakawa, H. (2010). Highly efficient plastic-substrate dye-sensitized solar cells with validated conversion efficiency of 7.6 %. *Solar Energy Materials and Solar Cells, 94*(5), 812–816.

Yum, J. H., Lee, J. W., Kim, Y., Humphry-Baker, R., Park, N. G., & Grätzel, M. (2014). Panchromatic light harvesting by dye-and quantum dot-sensitized solar cells. *Solar Energy, 109*, 183–188.

Zhuiykov, S. (2014). Nanostructured semiconductor composites for solar cells. In S. Zhuiykov (Ed.), *Nanostructured semiconductor oxides for the next generation of electronics and functional devices properties and applications* (pp. 267–320). Cambridge: Woodhead Publishing Limited.